Velocity Measurements of Airframe Effects on a Rotor in Low-Speed Forward Flight

S. G. Liou,* N. M. Komerath,† and H. M. McMahon‡
Georgia Institute of Technology, Atlanta, Georgia

Aerodynamic interactions between the rotor and the airframe of a rotorcraft can have severe effects and are difficult to predict analytically. To attack this problem, the velocity field of a two-bladed rotor has been measured in a wind tunnel with and without an airframe model in proximity. The periodic and time-averged velocity fields were measured using a laser velocimeter in planes both parallel to and above and below the rotor tip path plane at an advance ratio of 0.1 and a rotor tip Mach number of 0.29. The data were shown to be free of tunnel wall effects. The effect of including the cylindrical airframe model were measured. For the geometry studied, airframe influence on the rotor flowfield was mostly confined to the front half of the rotor disc. Hub effects were noticeable, even with the minimal-sized hub used. Strong vortex interaction effects were observed using strobed laser sheet flow visualization and measured using laser velocimetry.

Nomenclature

$a1$ = longitudinal flapping angle of rotor tip path plane. Positive when trailing edge of tip path plane is higher than leading edge
$b1$ = lateral flapping angle of rotor tip path plane. Positive when retreating side of rotor tip path plane is higher than advancing side
c = chord of rotor blade
H = vertical distance between airframe axis and rotor tip path plane
R = rotor radius
r = radial location
U = flow velocity component parallel to tunnel axis. Positive along tunnel freestream direction
U_∞ = tunnel freestream velocity
V = vertical component of velocity, positive downward
w = velocity component directed normal to rotor tip path plane, positive along rotor outflow direction (downward)
Δw = difference in measured values of w, found by subtracting the value with the airframe absent from that with the airframe present
X = coordinate direction parallel to tunnel axis. Origin at center of rotor hub pin
Xb = distance along airframe axis measured from airframe nose
Xn = distance along airframe axis measured from vertical line through rotor hub pin
Y = lateral axis. Origin at vertical plane through airframe axis
Y_{local} = value of Y, relative to the rotor blade tip, used to discuss vortex interaction effects
Z = vertical axis. Origin at center of rotor hub pin. Also, vertical displacement of rotor disc trailing edge for tip path plane determination
Z' = vertical displacement of the edge of the rotor disc at the retreating side, used in tip path plane determination
Z_{local} = value of Z, relative to the rotor blade quarter-chord line, at the edge of the rotor disc, used to discuss vortex interaction effects
μ = advance ratio. Ratio of tunnel freestream speed to rotor tip speed
θ = azimuthal location of measuring volume. Measured from freestream direction
Ψ = azimuthal location of quarter chord line of reference rotor blade. Measured from freestream direction. ($\Psi = 0$ at trailing edge of rotor)

Received Dec. 8, 1987; presented as Paper 88-0666 at the AIAA 26th Aerospace Sciences Meeting, Reno, NV, Jan. 11-14, 1988; revision received June 23, 1988.

*Graduate Research Assistant, School of Aerospace Engineering. Student Member AIAA.
†Assistant Professor, School of Aerospace Engineering. Member AIAA.
‡Professor, School of Aerospace Engineering. Senior Member AIAA.

Introduction

ROTORCRAFT in low-speed forward flight operate in three-dimensional, vortical flowfields. The wake of the main rotor contains strong vortices and vortex sheets and flows over the airframe. The resulting interactions cause complex and often unexpected effects that can seriously impair performance. Detailed knowledge of the flowfield is essential to make accurate predictions at the design stage. Current analytical codes can predict the performance of an isolated rotor or airframe quite satisfactorily but fail to give reliable predictions on the entire rotorcraft because of a lack of information on the physics of the interactions. The scarcity of detailed data hinders code validation. The objective of the present study is to gain a physical understanding of interaction phenomena to aid analytical modeling and also to provide a database on a simple configuration for validation of new codes.

Current design trends have made aerodynamic interaction problems more critical. Agility requirements dictate the use of shorter rotor masts as do the constraints imposed by the need to load small rotorcraft quickly on board large transport aircraft. Advanced gas turbine engines enable the use of rotors with lower aspect ratio and higher disc loading. Interactions can have benefits, as in reducing the need for a tail rotor. Sheridan and Smith[1] provided a systematic description of interactional aerodynamics, pointed to its growing importance,

and provided a framework for progress. Wilby et al.[2] studied the influence of the fuselage on rotor loads with different body shapes and mast heights, and concluded that the influence of the fuselage upwash is important and must be included in calculating blade and hub loads. Freeman and Wilson[3] studied the effects of several test parameters such as fuselage width, rotor-fuselage separation distance, and rotor thrust coefficient on the time-averaged fuselage surface pressure distribution. They showed that smaller rotor-fuselage separation distance, greater fuselage width, and thrust level increase the fuselage download. The effects were more pronounced under the front half of the rotor disc. Betzina et al.[4] used wind-tunnel tests to determine mutual interaction effects on different bodies under various conditions. They showed that the presence of a rotor and hub has significant effects on body aerodynamic characteristics. Egolf et al.[5] recently used a new analytical method to treat unsteady interactional aerodynamics between the rotor wake and fuselage. Their results agree well with data on mean and periodic surface pressure variations given by Brand et al.[6]

Some essential elements are common to all prediction codes for aerodynamic interactions. Schemes for predicting the pressure distributions of the rotor and the airframe are required and may be validated independently. Data on airframe surface pressure and rotor thrust are becoming available for these purposes. Schemes for predicting the effects of the rotor on the airframe and vice-versa are also required and, at the present state of technology, must proceed in an iterative manner. The interaction occurs through the flowfield, so that flowfield predictions are vital, in addition to surface pressure computations. Hence, the task of acquiring detailed velocity data was undertaken here. These complement a database on mean and fluctuating surface pressures[7] and on the vortex trajectories and dynamics.[8] The three-dimensional and unsteady nature of the flowfield, the presence of strong, curved vortices, as well as the need to make measurements close to the spinning rotor, make intrusive probes unsuitable for precise measurements. Thus, a laser velocimeter is used here. This offers the additional advantage of unambiguous resolution of the components of the local velocity. Only two components are measured extensively, these being the streamwise (U) and vertical (v) components, shown in Fig. 1b. Results from codes can be resolved into components, and can thus be compared.

Some previous studies have been performed using laser velocimetry on rotary wing configurations in forward flight. Biggers et al.,[9] Landgrebe et al.,[10] and Desopper et al.[11] performed various experiments that demonstrate this technique in such flowfields. Initial measurements on the present configuration were reported in Ref. 12. A series of experiments have been conducted recently at NASA Langley to determine the inflow above an isolated rotor.[13] The present work, however, is the first in the open literature to document both the inflow and the rotor wake velocity variations and to investigate the effect on the rotor flowfield of an airframe being present.

Facility Description

Figure 1 shows the test configuration. A cylindrical airframe model of 134 mm diam with a hemispherical nose is sting-mounted below a two-bladed teetering rotor. The rotor shaft is powered by a 3 hp electric motor mounted above the test section. The rotor and the airframe are linked solely through the flowfield, and their relative positions can be varied. The airframe is instrumented with 94 static pressure taps and 18 microphone ports. The rotor consists of two untwisted NACA 0015 blades of 86 mm chord rigidly attached to one another and mounted using a teetering pin assembly to the rotor shaft. The hub size is minimized by this design, at the expense of cyclic pitch control and flapping capability, to minimize contamination of the data by hub effects. The stiffness of the blades eliminates coning. The blades are preset at 10 deg collective pitch. The rotor diameter is 0.914 m, and the blade cord is 0.086 m. The shaft is tilted forward 6 deg to simulate the forward flight condition. The rotor speed was held constant at 2100 rpm. The advance ratio μ, defined as the ratio of the tunnel freestream velocity to the rotor tip speed, was varied by varying tunnel velocity.

Tunnel Flow Quality

The freestream turbulence intensity in the test section was found using both hot-wire anemometry and laser velocimetry to be lower than 1%. Tuft visualization studies verified that the wake of the rotor did not hit the tunnel floor in the test sec-

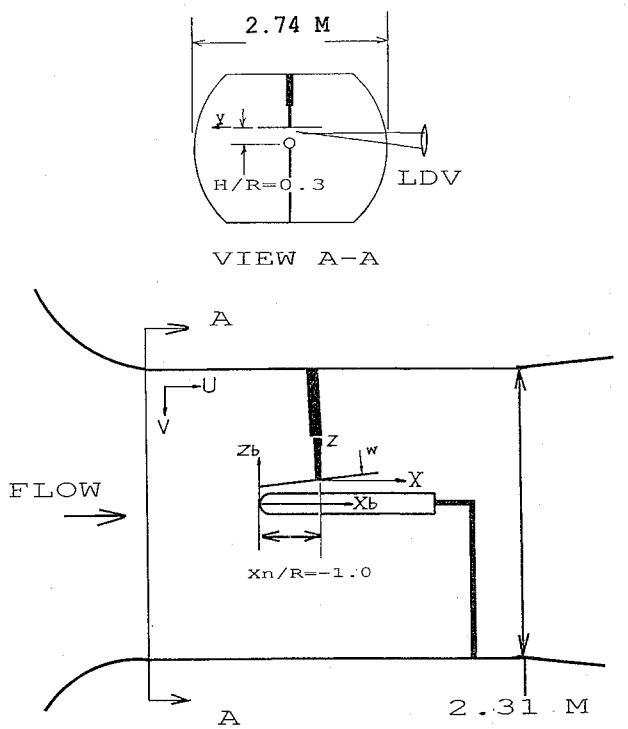

Fig. 1 Rotor-airframe configuration.

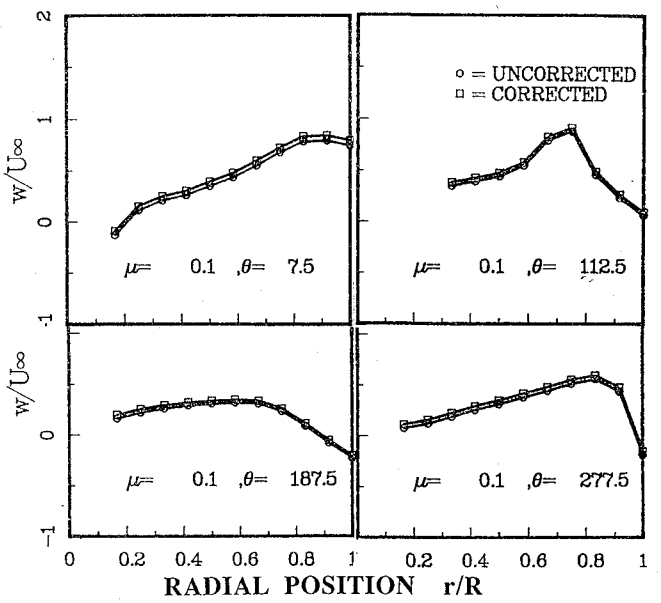

Fig. 2 Wind tunnel confinement effects on the measured time-averaged normal velocity along radial lines located 12.7 mm below the rotor disc. The circles are raw data; the squares are values corrected for confinement effects.

tion for advance ratios above 0.06. All data were acquired at advance ratios of 0.075 or higher. The influence of the tunnel floor and walls during powered lift experiments was checked using the methods of Heyson[14] and Hackett.[15] The effect of the tunnel floor was modeled by the method of images, and the blockage effects of the wake were taken into account. Heyson's program[16] was modified to calculate the interference factors for this configuration. The effect of including these correction factors was studied both as regards the mean airframe surface pressure data and the time-averaged velocity data acquired 12.7 mm below the rotor plane at various azimuth locations θ. The airframe pressure field was negligibly affected.[12] Figure 2 shows that the effects on the measured velocity field close to the rotor are negligible as well, for advanced ratios above 0.075. Thus, the velocity measurements presented here are essentially free of test section confinement effects.

Laser Velocimeter System

The laser Doppler velocimeter (LDV) used is a two-color, two-component system powered by a 5-W Argon ion laser. In the present tests, all data acquired were indexed to the rotor azimuth, and no cross-correlations between velocity components were sought. Hence, the LDV was operated as a single-component system to maximize signal quality and data rates and to minimize alignment time. The elimination of the color filters and beam steering modules required for two-component alignment resulted in a very large increase in the productivity of the system because the signal-to-noise ratio improved greatly. Light was collected in the backscatter mode. A Bragg Cell and variable frequency shifter were used to resolve flow direction. Two different lenses were used, with focal lengths of 1500 and 2186 mm, to permit complete coverage of the rotor-airframe configuration. The measurement volume of the LDV was translated in three dimensions using a computer-controlled optical traverse system. Seeding particles for the LDV measurement were generated downstream of the test section by atomizing mineral oil. Thus the seeded flow had to pass through the complete tunnel circuit before reaching the test section, resulting in a uniformly seeded flowfield in the test section. The surviving seed particles had extremely low settling rates. Details of the seeding scheme are reported in Ref. 12. Benchmark measurements were performed using hot-wire and pitot-static probes in the tunnel freestream. The mean velocity agreed to within 0.1%.

Synchronization

A trigger pulse was generated once per shaft revolution when the blade quarter-chord lines were aligned with the tunnel freestream. This happened because a notch in a ring mounted on the rotor shaft passed a light source, allowing light to be sensed by a photocell connected to a pulse amplifier and a shaping circuit. Experiments with a strobe driven by this signal showed that the delay involved was negligible. No correction was therefore made in the data for pulse delay. This signal was used to reset the time-between-data-points counter of the LDV signal processor interface. The analysis software thus related each data value to the rotor phase at the instant of data validation. The data were then sorted into azimuthal slots with 6 deg resolution to give the azimuth-resolved velocity variation. The data arriving during blade passage over the measuring location were further resolved into 32 bins, each usually of 0.5 deg resolution. The data acquisition and processing scheme is illustrated in Fig. 3. One drawback of this scheme is that data values collected before the first sync pulse in each block of data have to be discarded, as there is no way of determining their relation to rotor phase. This is not a problem at the data rates used here, as only a few points arrive during every rotor cycle. At high data rates, this will become a problem, whose solution is to acquire very large blocks of data.

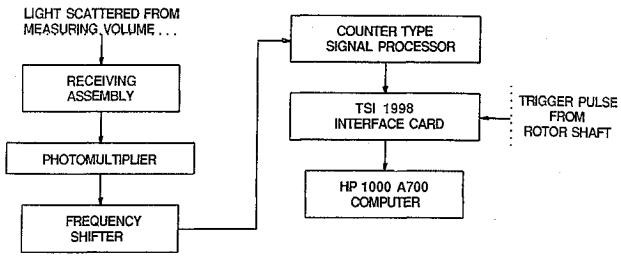

Fig. 3 LDV data acquisition and processing scheme.

Data Acquisition

At each measuring location, 60 blocks of data, each consisting of 500 individual velocity measurements, were taken. Each block was sorted into azimuth slots as indicated above. At the end of processing the 60th block, the value in each slot was ensemble-averaged. The time-averaged velocity at the measuring location was obtained by averaging the slot ensemble-averages. This procedure ensures that the velocity bias effect, where more data points are collected during intervals of high flow velocity, causes no error in the measurements.

Since large variations in velocity occurred, the frequency shift values and the filter settings on the counter processors had to be closely monitored and frequently changed to ensure accuracy. This limited the level of automation of the measurement procedures. The results at each location were displayed graphically and examined by the experimenter before the next measurement was started. This, combined with the fact that 30,000 velocity measurements were taken at each location, put severe constraints on the number of locations that could be studied. Typically, each component of velocity at each location required about 7 min of tunnel operation, of which 3 min went for moving to a location and acquiring and processing data, and 4 min for examining results on the monitor and storing files. The consistency of the results rewarded these stringent procedures, especially in the wake measurements.

Experiments

Tip-Path-Plane Determination

Since most of the measurements in this test were performed in planes parallel to the rotor tip path plane, the location of this plane had to be determined first. This was accomplished by measuring the longitudinal and lateral flapping angles. Figure 4 shows the geometrical relationships involved. These angles were determined by moving one of the beams of the LDV using the traverse until it touched the blade surface, a condition made visible by darkening the test section. The traverse counters were read to note position. The longitudinal flapping angles were 4.06 and 4.59 deg with the airframe present and absent, respectively, at $\mu = 0.1$, and the corresponding lateral flapping angles were 2.03 and 2.13 deg, respectively. These results proved repeatable to within 0.01 deg, with different operators performing the measurement. Once the tip path plane was determined, measuring locations were calculated using a coordinate transformation program, which transformed the required radial and azimuthal coordinates to traverse settings through a Jacobian operator. The results were used to move the measuring volume of the LDV remotely and to avoid obstructions in the beam paths.

Wake Measurements

The measuring plane was 12.7 mm below the blade trailing edge and was parallel to the tip path plane. A total of 212 locations, shown in Fig. 5a were studied. The baseline data set was acquired at an advance ratio of 0.1. The relative positions and separation distance of the rotor and airframe are shown in Fig. 1. Some measurements at an advance ratio of 0.15 were

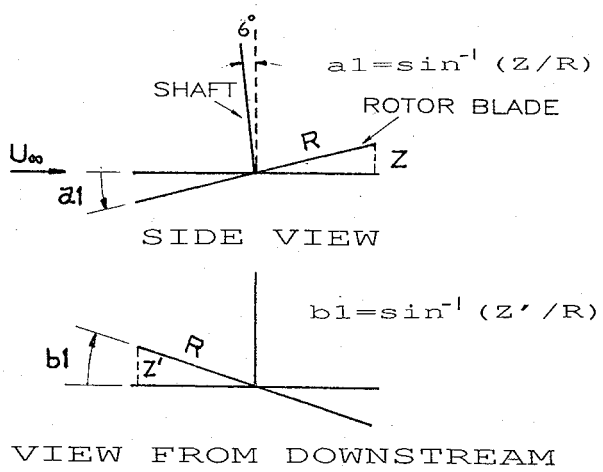

Fig. 4 Determination of the rotor tip path plane.

conducted in the second and third quadrants of the rotor plane with and without the body present for comparison purposes.

Because of the many obstructions caused by the tunnel force balance structure and the rotor shaft, the wake survey had to be conducted in several stages. The focusing lens had to be changed to enable complete coverage along the optical axis, and the LDV had to be moved to complete measurements over the forward part of the rotor disk. The traverse arms had to be tilted to send the beams over and under obstructions. In all this, it proved possible to keep the accuracy of the measurements high by using points on the hub and the rotor blade as references, and by performing the appropriate coordinate transformations. Repeatability of the velocity traces proved excellent.

Inflow Measurements

Rotor inflow was measured 12.7 mm above the tip path plane at the same operating conditions as outflow but at fewer locations. Several critical positions were chosen to study the effect of the body on inflow variation, as shown in Fig. 5b. It was found that inflow traces were quite smooth, as opposed to the sharp details seen in the wake, and posed no challenge to the measuring technique. The available tunnel time was used to concentrate on the wake rather than the inflow.

Laser Sheet Flow Visualization

The laser was also used as a source of illumination for flow visualization. In this mode, the full power of the laser was employed using a broadband mirror rather than a single-wavelength prism. The beam was passed through a Bragg Cell connected to a modulating circuit. A pulse generator was used to trigger the circuit, so that the laser beam was allowed to pass only for a short, controllable duration during every rotor cycle. The beam was expanded into a thin light sheet, which was used to illuminate desired cross sections. The seeded flow scattered sufficient light for videography, except from the highly accelerated vortex core regions, which showed up as dark spots with few scattering particles. By desynchronizing the pulse generator from the rotor slightly, it was possible to obtain a large video data base on the dynamics of the vortex-dominated flowfield. Figure 6 shows a photograph of a vortex core cross section, "frozen" just above the airframe. Such observations were used where necessary and possible to guide and interpret the LDV measurements. The flow visualization technique and results are discussed in detail in Ref. 8.

Results and Discussion

Repeatability

Figure 7 shows the azimuth-resolved velocity plots at one measuring point, in this case located at 2/3 of the rotor radius

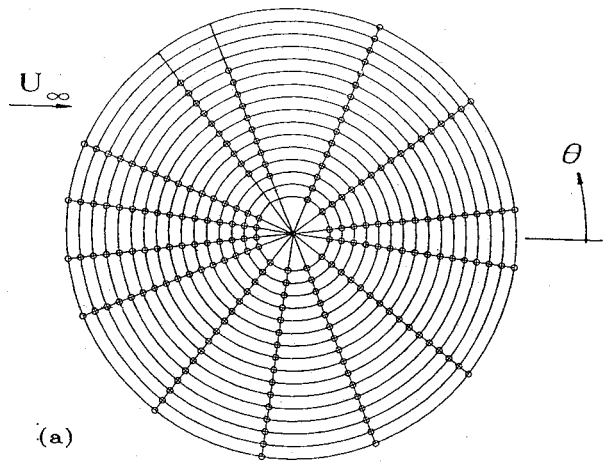

Fig. 5a Measuring locations in the wake.

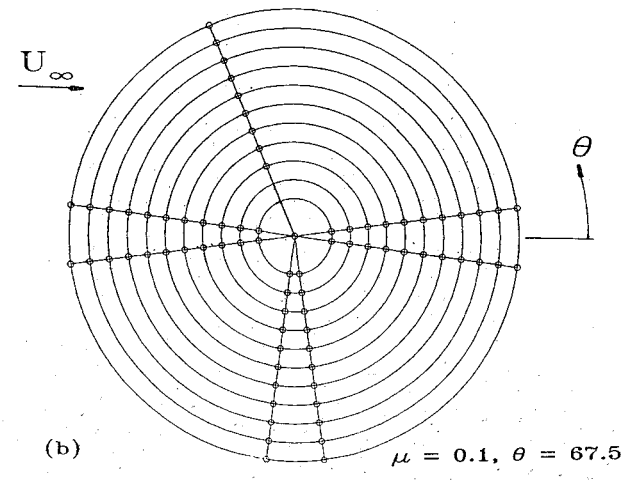

Fig. 5b Measuring locations in the inflow region.

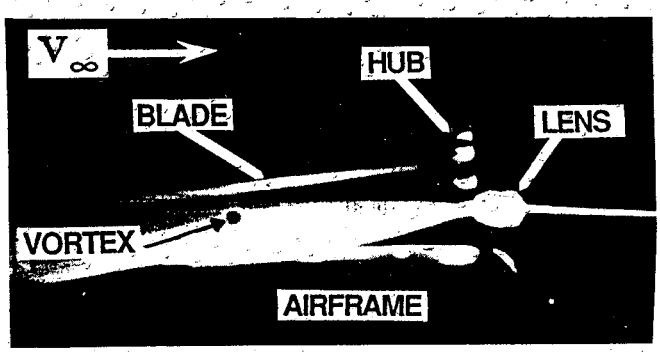

Fig. 6 Vortex core cross section "frozen" above airframe by a strobed laser sheet.

from the hub along the 67.5 deg azimuth line. The advance ratio was 0.1. The positive directions of the velocity components are shown in Fig. 1b. The presence of two blades provides a clear test of repeatability, which is very good, even at the sharp peaks of the periodic variation.

Inflow

The time-averaged inflow velocities normal to the rotor tip path plane, measured 12.7 mm above the rotor disk, are shown in Fig. 8, along radii at four selected azimuths. Downward velocities are shown positive, as before. Upflow is seen immediately downstream of the hub at 7.5 deg, and at out-

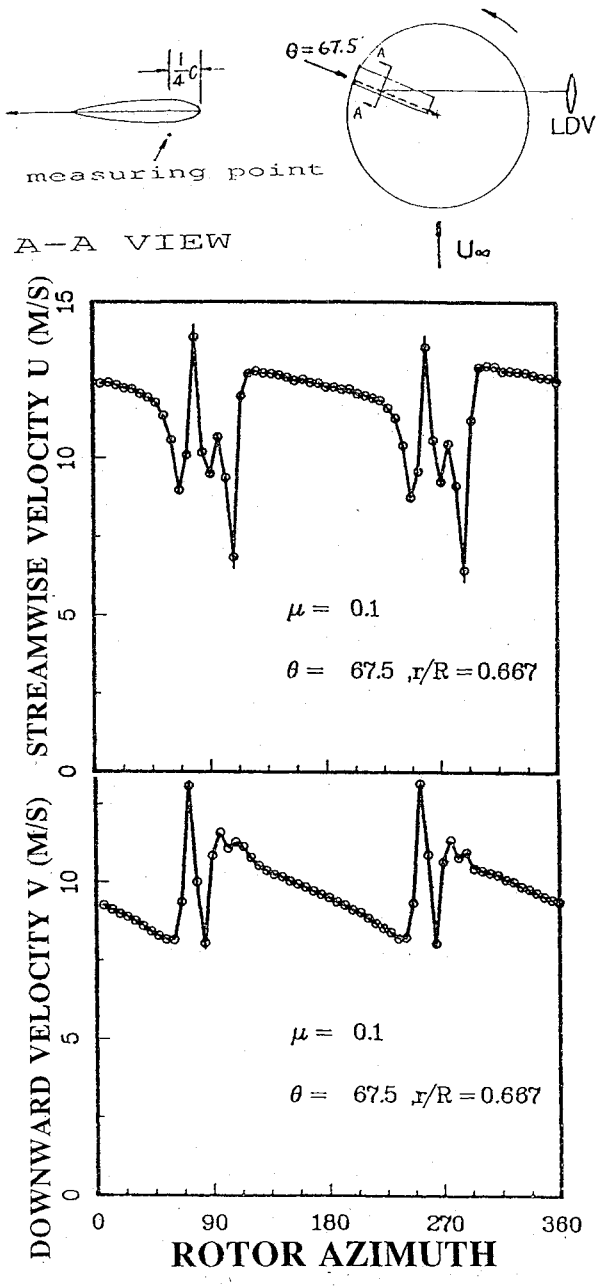

Fig. 7 Azimuth-resolved velocity components at $\theta = 67.5$ deg, measured 12.7 mm below rotor disc.

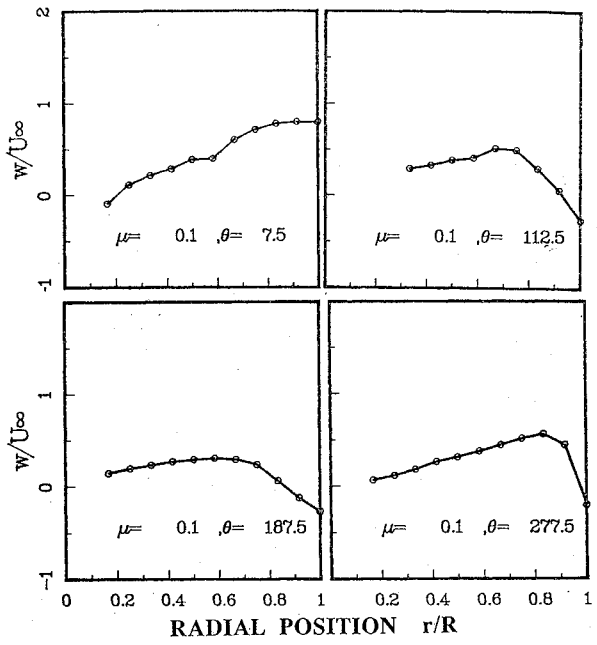

Fig. 8 Radial variations in inflow velocity, measured 12.5 mm above the rotor disc, at four representative azimuths.

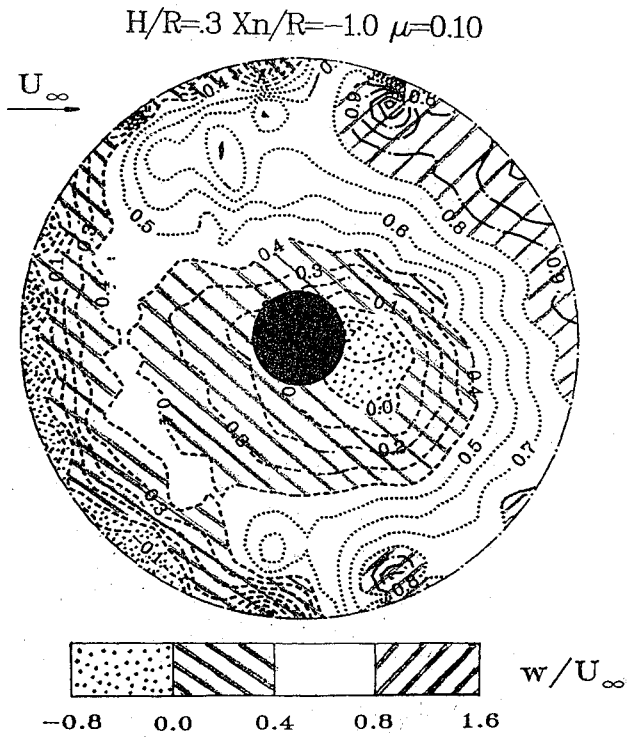

Fig. 9 Contour plot of the time-averaged downward velocity measured 12.7 mm below the rotor disc. Negative values denote upflow.

board locations at 112.5 and 187.5 deg. The character of the inflow distribution varies widely with azimuth, with sharp variations at 277.5 deg, and much gentler ones at 112.5, 187.5, and 7.5 deg. The inflow at the rear was much higher than in front except at a small region behind the hub, where the hub effect reduced the downward velocity. A smooth change from downflow to upflow occurred outboard of the blade at 187.5 deg, due to the effects of the body nose and tip vortex. At the advancing and retreating sides, sharp changes occur near the tip region, due to the strong tip vortex as in the outflow case.

Time-Averaged Flowfield Below Rotor Disc

The complexity of the rotor wake in forward flight can be seen from Fig. 9, which is a contour plot of the time-averaged velocity w normal to the tip path plane measured in the presence of the airframe. The values are normalized using the freestream velocity and are positive downward. The distribution is not symmetrical with respect to the longitudinal axis. The strongest downflow occurs around 70 and 290 deg, and between 25 and 45 deg. Upflow exists near the tip region throughout the front part of the disc. There is also a region of upflow downstream of the hub, which indicates a pronounced hub effect. This may be attributed to two causes: the flow separation downstream of the hub, and the rotation imparted to the flow by the viscous effects near the hub. Neither of these effects is easy to include in rotor flowfield prediction codes, and yet they may account for some of the disagreement found between predictions and measurement, as in Ref. 13 for example. The flowfield around 200 deg is also complicated by

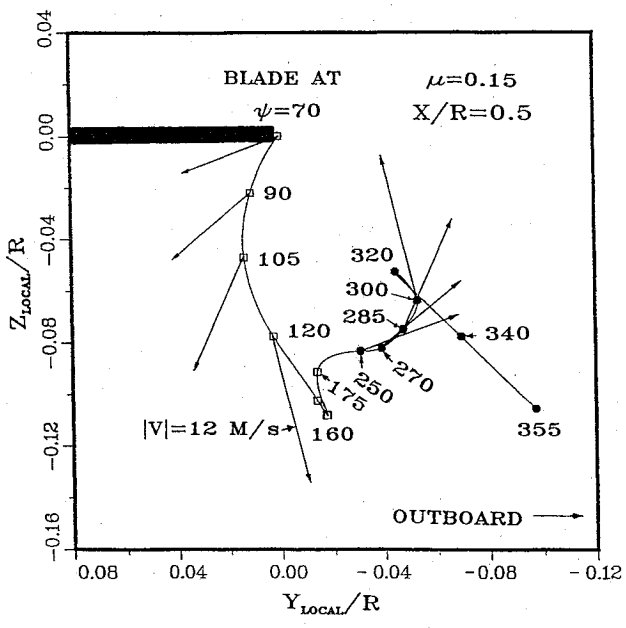

Fig. 10 Trajectory of a vortex pair near the outboard edge of the wake.[8]

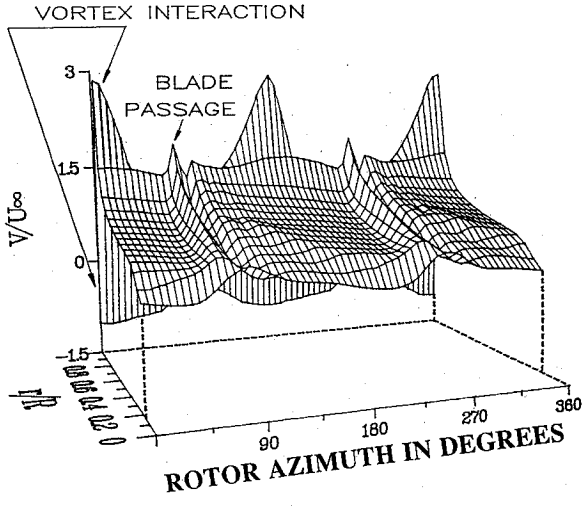

Fig. 11 Radial variation of the azimuth-resolved downward velocity at $\theta = 67.5$ deg, showing vortex interaction effects as large velocity variations occurring between blade passage events.

the severe tip vortex roll-up process in this region described by Spievy.[18] This causes sharp oscillations in contour lines. Downstream of the most outboard edges of the rotor (90 and 270 deg), two regions of very high velocity gradients are seen, located almost symmetrically about the longitudinal axis. These regions are where secondary vortex formation phenomena are observed. This phenomenon can be visualized by considering the rotor disc to be a low-aspect ratio wing, with wing-tip vortices rolling up.

Secondary Vortex Generation: An Observation

Near the azimuthal location shown in Fig. 7, the phenomenon of "secondary vortex generation," pointed out by Larin,[17] was noticed in the flow visualization data acquired by Brand et al.[8] At this location, the tip vortex spirals from the two blades were found to interact with each other, causing them to oscillate about one another in a periodic fashion. A pair of vortices appeared to leave and be convected downstream. This phenomenon is believed to be partly

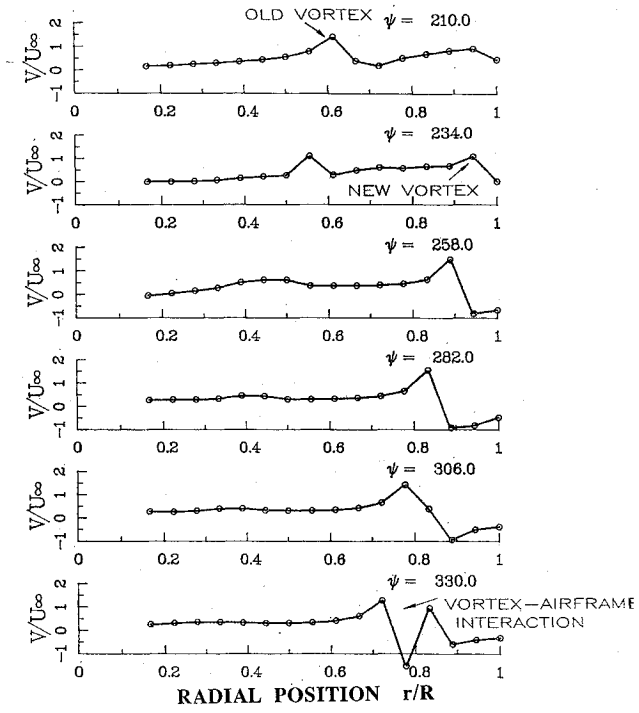

Fig. 12 Radial variations in the downward velocity at a sequence of rotor azimuths, measured at $\theta = 202.5$ deg, 12.7 mm below rotor disc.

responsible for the complex velocity variations seen in Fig. 7. Figure 10 from Ref. 8 is an attempt to provide a graphical description of such an event, although this was captured for a different rotor blade, at an advance ratio of 0.15. Closed symbols mark the observed locations of the old vortex at the rotor azimuths indicated. Open symbols show the motion of the new vortex. Note that all the azimuth numbers are referenced to the position of the blade shedding the new vortex. The velocities induced at the center of the core of each vortex is indicated by a vector, which is approximately calculated from the observed trajectories in the video data base. A satisfactory explanation has not yet been possible for the observed discontinuities in the trajectory; these must be attributed to close interaction between neighboring vortex filaments. The observed "break-off" and convection of secondary vortex structures has not been shown. The variations in the periodic velocity along the radius are shown in Fig. 11. It is seen that the vortex interaction effects are pronounced toward the blade tips, where a very large excursion in the downward velocity occurs. A detailed and consistent explanation of this phenomenon must await further detailed studies.

Close Vortex Interaction Effects on the Instantaneous Induced Velocity

Figure 12 shows what happens along the radius at an azimuth of 202.5 deg as the blade moves away from 210 to 330 deg. The peak downward velocity, which corresponds to the tip vortex spiral, moves inboard as the vortex sinks toward the airframe surface. A second peak appears due to a new vortex moving inboard. Flow visualization shows this vortex reaching the airframe at about 260 deg. At about 318 deg blade azimuth, two velocity peaks appear, indicating a dramatic change in the vortex. This corresponds to the disappearance of the vortex core in the laser sheet visualization data. This is believed to be due to the airframe effect on the vortex, with the vortex sheet being forced away from the tip vortex core, and the core weakening considerably.

The geometry of the tip vortices was computed using the free wake code developed by Scully.[19] This vortex geometry is

compared with the observed velocity variations below the rotor disc with the blade at 270 deg in Fig. 13. Both the computed and experimental results shown are for an instant (a 6-deg interval, in the case of the measured data) when the two blades are perpendicular to the flight direction. The experimental velocity profiles in Fig. 13a show large "blips" involving a change in sign, typical of vortex passage, at locations corresponding to the computed locations of the vortex spirals in Fig. 13b. As expected, vortex passage drastically modifies the induced velocity close to the edge of the rotor disc when the measurement location is in the third quadrant, since the vortex from the previous blade is convected downstream and inboard. The velocity profiles acquired for measurement locations between 330 and 120 deg show no such "blips." The vortex in question is outboard of the edge of the rotor disc for these locations. One of the difficulties in comparing theory and experiment is seen in this figure. The free wake code gives the wake geometry at an instant when the blades are at a particular azimuthal orientation, in this case the 270-90 deg diam. The experimental data obtained over the whole disc have to be sorted to extract the occurrences at each azimuthal and radial position when the blades were at this orientation.

Airframe Effects

The effects of the airframe on the measured wake velocities near the rotor plane were gaged by subtracting the time-averaged velocities normal to the rotor tip path plane obtained without the airframe present from those with the airframe present. The results are shown in Fig. 14. The differences in w are seen to be of the same order as w itself. The major effects are felt over a crescent over the front half of the rotor disc, and along a narrow strip along the streamwise diameter. These

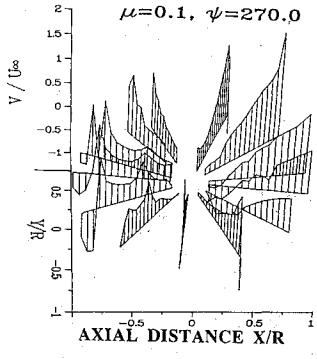

Fig. 13a Radial variations in induced velocity at an instant when the rotor blades are perpendicular to the freestream, showing sharp variations inboard of the edge of the disc due to close vortex passage.

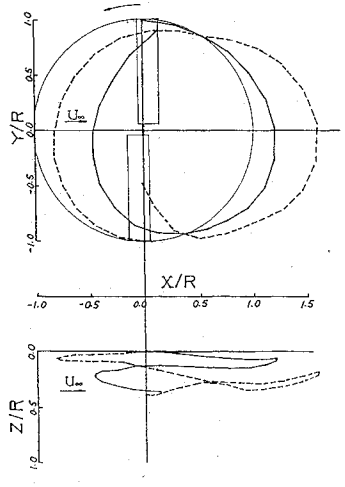

Fig. 13b Vortex trajectories computed from the free wake code of Ref. 19, showing the vortex filaments at this instant.

effects can be explained as follows. The airframe causes an upflow (dip) about the front of the airframe, especially at the leading edge of the disc. This can also be explained in terms of displacement of the vortex trajectories. There is also an asymmetry introduced by the airframe. Thus, sharp peaks and valleys are seen in close proximity, corresponding to displacement of vortices; these occur asymmetrically on either side of the airframe. In general, away from the airframe the presence of the airframe causes no large effects. This may be particular to the airframe shape used. Effects at the rear half of the rotor disc are quite small. This result is unique since it shows the difference caused to the rotor flowfield by the airframe alone, exclusive of the rotor hub and mast. The narrow region of increased upflow along the streamwise diameter is due to the close vicinity of the top of the airframe, which blocks the downward flow that would otherwise exist here. As mentioned before, the hub and mast produce significant deviations from the "isolated rotor" analytical models in current use, and these cannot be separated from airframe effects except by using a configuration such as this one where the rotor is mounted independently of the airframe.

Vortex Passage

In Fig. 15, the effects of the airframe on the rotor flowfield at the front of the disc are shown using the periodic variation of the downward velocity at a location close to the blade tip. The first peak at about 0 and 180 deg corresponds to the thickness effect of each blade as it passes. The large excursion in velocity following these is due to the convection of a vortex. The variations in the figure are real, being repeatable from blade to blade. There are significant differences in magnitude, caused by the presence of the airframe. These are attributable to the displacement of the vortex trajectory by the airframe. More curious is the existence of two or three points where the downward velocity is zero, in the trace with the airframe present. These, on close examination of the raw data, were revealed to be due to the passage of the inner core of the vortex. Inside the inner core, the probability of findings a seed particle is extremely low. Since the number of particles sensed was zero, the velocity could not be measured at these points. Thus, the velocity at these points is artificially set to zero relative to the measuring point. The upflow occurring between 90 and 200 deg is greater with the airframe present, since this location is close to the nose of the airframe. Figure 16 shows the downward velocity further inboard at the same azimuth. The

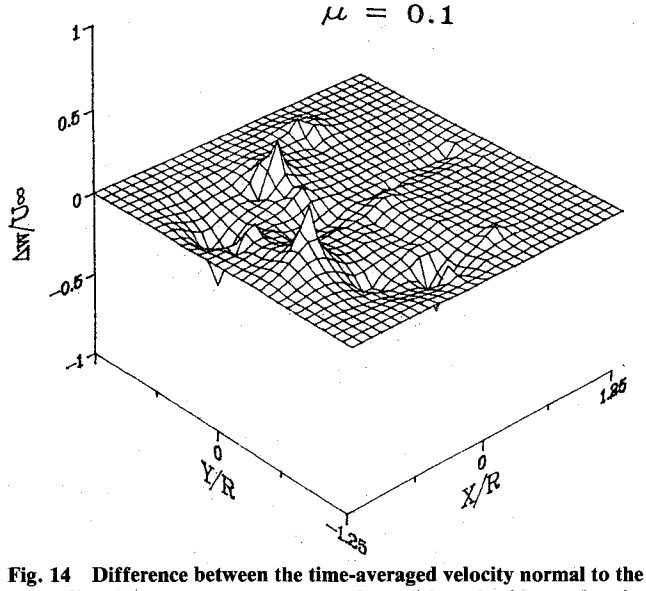

Fig. 14 Difference between the time-averaged velocity normal to the rotor disc, between measurements taken with and without the airframe present.

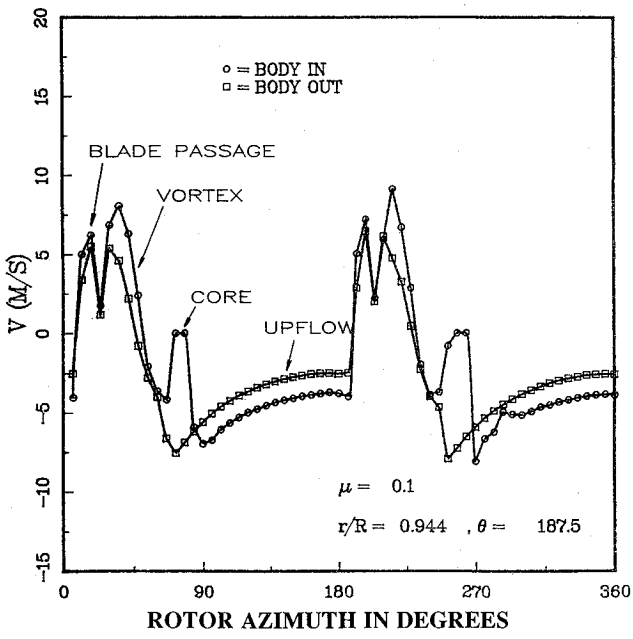

Fig. 15 Periodic variation of outflow near the leading edge of the rotor disc, showing airframe effects on vortex roll-up.

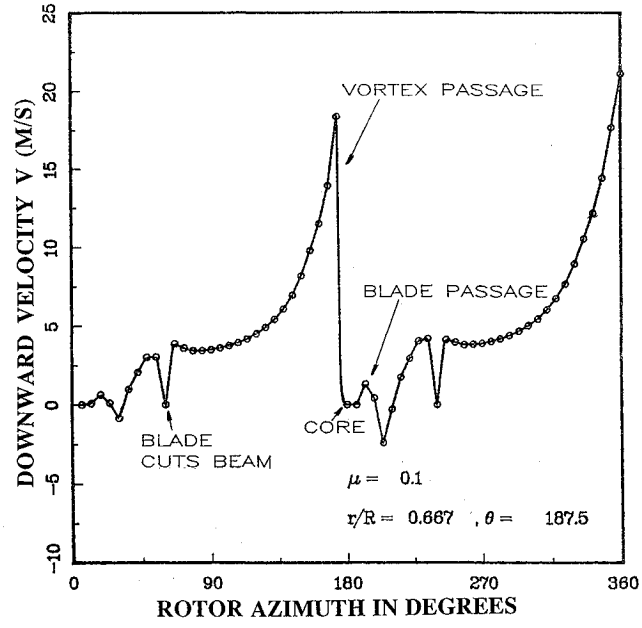

Fig. 16 Periodic variation of outflow 1/3 R inboard of the leading edge, showing the effects of passage of a fully developed vortex as well as the roll-up process.

small dips to zero velocity here are again because there are no seed particles sensed at these azimuths. However, this is for a different reason: for a brief instant during each revolution, the bottom of the blade intersects one of the laser beams at this location. Again, the software filters eliminate data obtained at these instants and prevent them from being counted as fluid velocity. The large excursions are again due to vortex passage, this time the passage of the strong fully developed vortex from the previous blade. Again, there are points of zero velocity in the core, where no velocity could be measured because of the lack of seed particles. The thickness effect of the blade passage is smaller now, because the tangential velocity of the blade is smaller than at the tip.

The effects of the airframe on the inflow were seen to be minimal and hence are not plotted here. Also, the presence of the airframe appears to cause only small differences in the flowfield away from the close vicinity of the airframe. These results are not entirely typical of existing rotorcraft. The airframe used here is proportionately larger in relation to the rotor than typical rotorcraft fuselages. However, this idealized airframe is more aerodynamically "streamlined" than a practical rotorcraft. This has one important implication: this test case can be used quite easily in the initial stages of development of an interaction code. Large-scale separation effects and complex airframe shapes can be easily introduced in the experiment, but they can be adequately dealt with only after this case becomes predictable.

Concluding Remarks

An extensive set of measurements has been acquired on the velocity field of a rotor in forward flight. Several features have been observed.

1) The inflow and wake have been measured in the close vicinity of the rotor, with and without an airframe present. The effects of the presence of the airframe on the rotor velocity field have been isolated and are seen to be as large in magnitude as the rotor-induced velocity itself. The airframe effects are mostly confined to the front of the disc and are mostly due to vortex displacement. Along the top of the airframe, downward velocity is reduced by airframe blockage.

2) Deviations from periodicity were negligible, as were the confinement effects of the wind tunnel, at the advance ratios used in the study. The data acquired proved to be consistent and repeatable with excellent accuracy, even in the near wake of the rotor, and in regions of strong vortex interactions.

3) The inflow to the rotor shows much smoother radial variations than does the wake, but the radial variation patterns depend strongly on azimuth.

4) The effects of the airframe itself on the rotor inflow are quite small for the idealized airframe studied here, so that an interaction calculation can reasonably be started with an isolated rotor calculation.

5) Even with a very small hub and a thin rotor mast, the effects of these features on the rotor flowfield are quite significant. In the current study, these effects have been separated from airframe effects.

6) Strong vortex interaction effects are present in the flowfield. There appears to be a vortex roll-up and shedding process similar to that on a low-aspect ratio wing at the outboard edges of the rotor disc. Vortex interaction with the airframe causes changes in the velocity pattern at the rotor.

Acknowledgments

The authors gratefully acknowledge the assistance of Albert Brand, who amassed the flow visualization data used to interpret many features of the velocity field, and of Dimitris Mavris, who obtained results using the Scully Free Wake code for comparison. This work was sponsored by the U.S. Army Research Office under Contract DAAG29-82-K-0084, the Center of Excellence in Rotary Wing Aircraft Technology program. Drs. Robert E. Singleton and Thomas Doligalski are the Technical Monitors.

References

[1]Sheridan, P. F. and Smith, R. P., "Interactional Aerodynamics—A New Challenge of Helicopter Technology," *Proceedings of the 35th Annual National Forum of the American Helicopter Society,* Washington, D.C., 1979, Paper 79-50.

[2]Wilby, P. G., Young, C., and Grant, J., "An Investigation of the Influence of Fuselage Flow Field on Rotor Loads and the Effects of Vehicle Configuration," *Vertica,* Vol. 3, 1979, pp. 79-94.

[3]Freeman, C. E. and Wilson,J. C., "Rotor-Body Interference (ROBIN)—Analysis and Test," *Proceedings of the 36th Annual National Forum of the American Helicopter Society,* Washington, D.C., 1980,Paper 80-5.

[4]Betzina, M. D., Smith, C. A., and Shinoda, P., "Rotor/Body Aerodynamic Interactions," *Vertica,* Vol. 9, No. 1, 1985, pp. 65-81.

[5]Egolf, T. A. and Lorber, P. F., "An Unsteady Rotor/Fuselage Interaction Method," *Proceedings of the American Helicopter Society, Specialists' Meeting on Aerodynamics and Aeroacoustics,* Washington, D.C., 1987.

[6]Brand, A. G., McMahon, H. M., and Komerath, N. M., "Surface Pressure Measurements on a Rotor-Airframe Configuration in Forward Flight," to appear in the *AIAA Journal.*

[7]Brand, A. G., McMahon, H. M., and Komerath, N. M., "Wind Tunnel Data From a Rotor Wake/Airframe Interaction Study," *CERWAT Data Report No. GITAER 87-1,* School of Aerospace Engineering, Georgia Institute of Technology, July 1986.

[8]Brand, A. G., Komerath, N. M., and McMahon, H. M., "Results from Laser Sheet Visualization of an Incompressible Vortex Wake," AIAA Paper 88-0192, Jan. 1988.

[9]Biggers, J. C. and Orloff, K. L., "Laser Velocimeter Measurements of the Helicopter Rotor-Induced Flow Field," *Journal of the American Helicopter Society,* Vol. 20, Jan. 1975, pp. 2–10.

[10]Landgrebe, A. J. and Johnson, B. V., "Measurement of Model Helicopter Rotor Flow Velocities with a Laser Doppler Velocimeter," *Journal of the American Helicopter Society,* Vol. 19, July 1974, pp. 39–43.

[11]Desopper, A., "Rotor Wake Measurements for a Rotor in Forward Flight," Office National d'Etudes et de Researches Aeronautiques, TP No-12, 1985.

[12]McMahon, H. M., Komerath, N. M., and Hubbartt, J. E., "Studies of Rotor-Airframe Aerodynamic Interactions in Forward Flight," AIAA Paper 85-5015, Oct. 1985.

[13]Elliott, J. W., Althoff, S. L., Sellers, W. L., and Nichols, C. E., Jr., "Inflow Velocity Measurements Made on a Helicopter Rotor Using a Two-Component Laser Velocimeter," AIAA Paper 87-1321, June 1987.

[14]Heyson, H. H., "Linearized Theory of Wind-Tunnel Jet-Boundary Corrections and Ground Effect for VTOL-STOL Aicraft," NASA TR R-124, 1962.

[15]Hackett, J. E., Wilsden, D. J., and Lilley, D. E., "Estimation of Tunnel Blockage from Wall Pressure Signatures: A Review and Data Correlation," NASA CR-152,241, March 1979.

[16]Heyson, H. H., "FORTRAN Programs for Calculating Wind-Tunnel Boundary Interference," NASA TM X-1740, 1969.

[17]Larin, A., "Vortex Wake Behind a Helicopter," Aviatsiya i Kosmonavtika, 3, 1973, pp. 32–33 (translated from Russian.)

[18]Spievy, R. F., "Blade Tip Aerodynamics-Profile and Planform Effects," *Proceedings of 24th Annual National Forum of the American Helicopter Society,* Washington, D.C., 1968, Paper 205.

[19]Scully, M. P., "Computation of Helicopter Rotor Wake Geometry and Its Influence on Rotor Harmonic Airloads," Aeroelastic and Structures Research Lab. Rept. 178-1, Massachusetts Institute of Technology, Cambridge, March 1975.